

Towards a Deep Unified Framework for Nuclear Reactor Perturbation Analysis

Fabio De Sousa Ribeiro*
and Francesco Calivá*
University of Lincoln
Lincoln, UK
{fdesousaribeiro, fcaliva}
@lincoln.ac.uk

Dionysios Chionis
and Abdelhamid Dokhane
Paul Scherrer Institute
Villigen, Switzerland
{dionysios.chionis,
abdelhamid.dokhane}@psi.ch

Antonios Mylonakis
and Christophe Demazière
Chalmers University
Gothenburg, Sweden
{antmyl, demaz}
@chalmers.se

Georgios Leontidis
and Stefanos Kollias
University of Lincoln
Lincoln, UK
{gleontidis, skollias}
@lincoln.ac.uk

Abstract—This paper proposes the first step towards a novel unified framework for the analysis of perturbations occurring in nuclear reactors in both Time and Frequency domain. The identification of type and source of such perturbations is fundamental for monitoring core reactors and guarantee safety even while running at nominal conditions. A 3D Convolutional Neural Network (3D-CNN) was employed to analyse perturbations happening in the frequency domain, such as the alteration of an absorber of variable strength or propagating perturbation. Recurrent neural networks (RNN), specifically Long Short-Term Memory (LSTM) was used to study signal sequences related to perturbations induced in the time domain, including the vibrations of fuel assemblies and the fluctuation of thermal-hydraulic parameters at the inlet of the reactor coolant loops. 512-dimensional representations were extracted from the 3D-CNN and LSTM architectures, and used as input to a fused multi-sigmoid classification layer to recognise the perturbation type. If the perturbation is frequency domain related, a separate fully-connected layer utilises said representations to regress the coordinates of its source. The results showed that perturbation type can be recognised with high accuracy in both domains, and frequency domain scenario sources can be localised with high precision.

Index Terms—deep learning, 3D convolutional neural networks, recurrent neural networks, long short-term memory, multilabel classification, regression, signal processing, nuclear reactors, unfolding, anomaly detection.

I. INTRODUCTION

For over half a century, the nuclear industry has primarily focused on the technological evolution of reliable nuclear power plants for the production of electricity. By monitoring nuclear reactors whilst running at nominal conditions, it is possible to gather valuable insight for early detection of anomalies. Various types of fluctuations can be caused by the turbulent nature of flow in the core, mechanical vibrations within the reactor, the boiling coolant and stochastic character of nuclear reactions, among other factors. These fluctuations are regarded as neutron noise $\delta X(\mathbf{r}, t)$, which is measured as in (1), where $X(\mathbf{r}, t)$ represents the signal and $X_0(\mathbf{r}, t)$ its trend. Both are a function of two variables: \mathbf{r} the spatial coordinate within the core, and t time.

$$\delta X(\mathbf{r}, t) = X(\mathbf{r}, t) - X_0(\mathbf{r}, t) \quad (1)$$

*Both authors contributed equally.

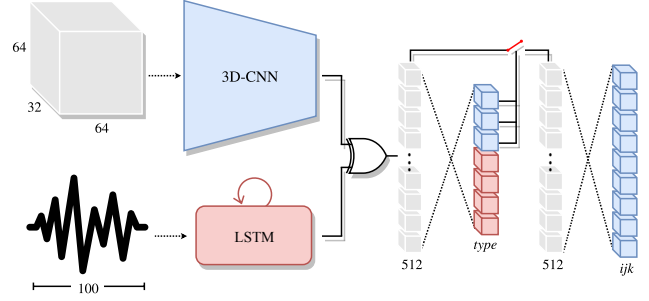


Fig. 1. Unified framework for Time and Frequency domain perturbation type classification and coordinate regression.

With detailed descriptions of reactor geometry, physical perturbations and probabilities of neutron interactions within the core - by assuming a particular reactor transfer function (i.e. Green's function) - one can simulate how fluctuations affect the neutron flux in the time or frequency domain. Different types of perturbations can then be applied in order to estimate and study the induced neutron noise, as to solve the *forward problem*. Intuitively, the *backward problem*, also known as *unfolding*, consists of localising the perturbation origin and can only be retrieved if the reactor transfer function is inverted. Solving the unfolding problem is therefore non-trivial as measurements of the induced neutron noise are not available at every position inside the reactor core, due to a limited number of in and out-core sensors available.

In this work, a novel method to unfold nuclear reactor signals pertaining to localisation of different types of induced perturbations is proposed. This is achieved by extending and improving previous research on the application of deep learning techniques to detect anomalies in nuclear reactors [1].

II. RELATED WORK

Fault detection in nuclear reactors has been the focus of a few recent studies. [2] proposed a pattern recognition framework to detect anomalies based on symbolic dynamic filtering of sensor time series data. [3] predicted critical heat flux by ways of Adaptive Neuro-Fuzzy Inference Systems. [4]

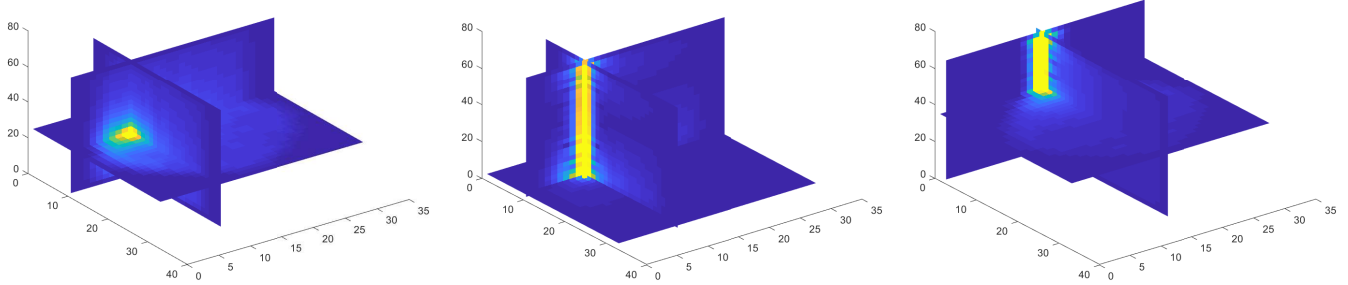


Fig. 2. Example of Perturbation Types. From **Left** to **right**: *Localised*, *Propagating* type 1 and 2.

monitored sensors by utilising auto-associative kernel regression and sequential probability ratio tests. [5] collected reactors parameters and implemented an artificial neural network based system to diagnose transients. [6] proposed a nuclear reactor fault detector based on the combination of principal component analysis and fisher discriminant analysis. Given the outburst in popularity of deep learning, a vast amount of research has recently been published presenting new techniques and approaches ([7]–[13]). In [14], a Convolutional Neural Network (CNN) and Naïve Bayes data fusion scheme was proposed for the detection of fractures in plant components by way of individual video frame analysis. In recent work by [1], a CNN was employed to localise the origin of perturbations in reactor core complex signals, which were simulated in the frequency domain. This was achieved by spatially splitting the signal voxels into 12 or 48 individual blocks, each pertaining to a different class. A classification task was then formulated, followed by a combination of k -means and k -NN based analysis of extracted latent variables, enabling a finer unfolding resolution of perturbation sources. Although the results were promising, an unfounded conversion of complex signal voxels for use in conventional CNNs led to unnecessary loss of spatial information. To address this limitation, in this work we propose a new bespoke 3D CNN model for multi-task perturbation unfolding regression and type classification. Additionally, we extend our analysis to time-domain simulated signals regarding excessively vibrating fuel assemblies and/or alteration of thermal-hydraulic parameters (e.g. inlet coolant flow and/or temperature).

III. THE EXAMINED SCENARIOS

A. Frequency Domain

In this study, CORE-SIM [15] was employed to model the induced neutron noise, in a Pressurised Water Reactor (PWR), under two scenario settings: *Absorber of Variable Strength* and a *Propagating Perturbation* in the frequency domain. During the forward problem, the reactor transfer function, which is considered to be the Green’s function of the system, captures the response of the induced neutron flux. The effect of a perturbation can be assessed from any spatial point within the core reactor, provided that there exist a one-to-one relationship between every possible location where a

perturbation is sourced and the position where the neutron noise is measured. The latter is described as:

$$\partial\phi(\mathbf{r}, \omega) = \int_V G(\mathbf{r}, \mathbf{r}_p, \omega) dS(\mathbf{r}_p) d\mathbf{r}_p \quad (2)$$

where the core transfer function is integrated across the whole core reactor volume V , whereas \mathbf{r}_p and ω refer to the source and the angular frequency of the perturbation respectively. For more details, please refer to the official CORE-SIM user manual [15], [16]. Diffusion theory was applied to perform a low-order approximation of the neutron flux angular moment. The energy of the system was discretised with a two-energy group formulation: one with a high and one low energy spectrum, henceforth referred to as the *Fast* and the *Thermal* groups respectively.

Absorber of Variable Strength: In this scenario (*Localised*, see Fig. 2), the thermal macroscopic absorption cross-section was perturbed at three different frequencies 0.1, 1 and 10 Hz, altering the absorption of thermal neutrons. This perturbation type can be considered as localised at a specific source location. A PWR with a radial core of size 15×15 fuel assemblies (FA) was modelled, using a volumetric mesh with $32 \times 32 \times 26$ voxels.

Propagating Perturbation: In these scenarios (*Propagating* type 1 and 2, see Fig. 2), fuel assemblies were also perturbed at 0.1, 1 and 10 Hz, with which the neutron noise fluctuations were modelled. Propagating perturbations were sourced either outside the core reactor and transported upwards with the coolant starting from the lowest level of the core (type 1); or within the core and propagated along the fuel assembly’s cross-section, by means of the coolant flow (type 2). Identical mesh specifications to the *Absorber of Variable Strength* scenario were adopted.

Combined Perturbations: In this scenario, combinations of the aforementioned perturbation types can occur simultaneously at different locations in the reactor. However, no more than one instance per perturbation type may occur at any given time.

Data Pre-processing: The complex signals are a 3D representation of the distribution of the induced neutron noise, including *Fast* and *Thermal* neutron groups. They are distributed in the form of voxels of size $32 \times 32 \times 26$, each containing

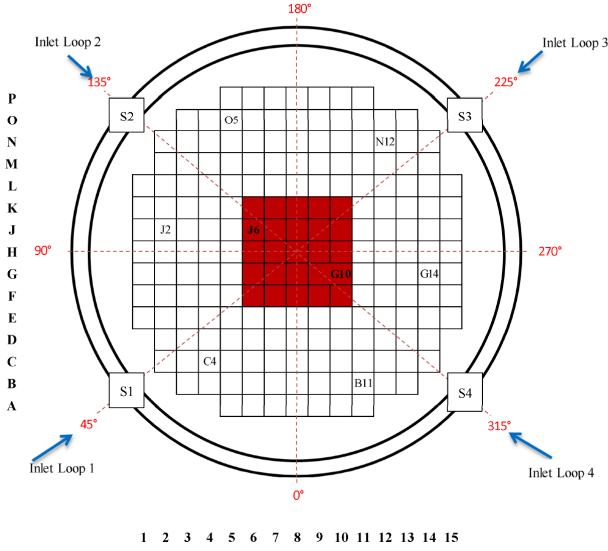


Fig. 3. Radial view of the core model utilised for the simulation with S3K.

a perturbation sourced at a specific coordinate location i, j, k (considered the label). The dataset is comprised of 19552 (*Absorber of Variable Strength*) and 752 (*Propagating type 1 and 2*) instances per frequency (0.1, 1 and 10 Hz). Furthermore, the signal was corrupted by obscuring parts (set values to zero) at random in order to emulate fewer available sensor measurements. Two versions of obscured data were generated with channel-wise repeated masks of size $32 \times 32 \times 26$. Each 32×32 mask was generated by randomly selecting 5% and 20% of measurements respectively, and setting remaining values to zero. As previously alluded to, a given reactor signal is composed of 2 types of responses, *Fast* and *Thermal*, each comprised of amplitude and phase. Resulting in a total of 4 components of size $32 \times 32 \times 26$, which we concatenated into a voxel of $64 \times 64 \times 26$, zero-padded to $64 \times 64 \times 32$ for training.

B. Time Domain

Simulate-3K (S3K) was utilised to model fuel assemblies cluster vibrations, including alterations of thermal-hydraulic parameters between the coolant loops, on a core model of the four-loop Westinghouse PWR mixed core, utilised in [17]. The system operating conditions were the same to those assumed in the frequency domain experiments. For more details with regard to S3K, the reader is encouraged to refer to the manual [18]. Fig. 3 depicts a cross-sectional view of the utilised core. The cluster of fuel assemblies is highlighted in red, whereas the coordinates (e.g. B11) identify the location of neutron detectors. The reactor is comprised of six axial levels and a total of fifty-six detectors: eight located ex-core, identically distributed at two axial levels (level 1 (*L1*) and level 6 (*L6*)); forty-eight in-core, equally distributed across the six levels. Every scenario had duration of 100s and it was sampled with time steps of 0.01s.

TABLE I
SYNCHRONISED VIBRATION OF A 5×5 FUEL ASSEMBLIES CENTRAL CLUSTER.

Scenario	Perturbation	Frequency	Amplitude	ID
1	5×5 cluster FAs	WN	1mm	1 0 0 0
	5×5 cluster FAs	WN	0.5mm	1 0 0 0
2	5×5 cluster FAs	1Hz	1mm	0 1 0 0
	5×5 cluster FAs	1Hz	0.5mm	0 1 0 0

TABLE II
SYNCHRONISED PERTURBATION OF COOLANT THERMAL-HYDRAULIC PARAMETERS.

Scenario	Perturbation	Frequency	Amplitude	ID
3	temperature	random	$\pm 1^\circ C$	0 0 1 0
4	flow	random	$\pm 1\%$	0 0 0 1

1) *Vibrating central cluster of fuel assemblies*: This perturbation refers to four scenarios (see Table I), in which a cluster of 5×5 fuel assemblies is vibrating synchronously in the x-direction, following either a white noise signal or a sine wave function ($f = 0.1Hz$), with varying amplitudes in the range of 0.5mm, and 1mm. "Binary ID" is a label later utilised to classify different perturbation types. It is worth noting that the first and second scenarios, same as the third and the fourth ones, essentially represent same scenarios respectively, since the applied perturbations are the same but with different amplitude. Therefore, two differing "individual" classes were identified out of the four scenarios.

2) *Perturbation of thermal-hydraulic parameters*: This perturbation refers to two scenarios, in which synchronised fluctuations of inlet coolant temperature between the four coolant loops were induced. As reported in Table II, the inlet coolant temperature was forced to fluctuate with amplitude of $\pm 1^\circ C$ over the mean value of $283.8^\circ C$ (third scenario). In the fourth scenario, inlet coolant flow random fluctuations with amplitude of 1% over the relative flow (100%) were simulated.

3) *Previous scenarios combination*: Scenarios five to thirteen refer to combinations of previous perturbations associated to the vibration of a 5×5 fuel assembly and fluctuations of inlet coolant thermal-hydraulic parameters between the four coolant loops. A detailed description of these scenarios is provided in Table III. In the column "Combination of perturbations", the number between brackets links to the Scenario ID reported in Table I and II.

Data Pre-processing: Signals produced by S3K are a representation of the neutron flux measured by the in-core and ex-core detectors. Taking into account duration of each applied perturbation and sampling rate, data from each sensor were available in the format of a vector of 10001 elements. Given the limited amount of data available, it was appropriate to perform data augmentation. With this purpose, each signal was re-sampled by means of sliding windows of 100 time-steps, using 5 time-steps stride, as shown in Fig. 4. Furthermore, the signal was corrupted by the addition of White Gaussian noise at signal-to-noise ratios $SNR = 10$ and 5 (Fig. 5).

TABLE III
COMBINATION OF SYNCHRONISED VIBRATION OF A 5×5 FUEL
ASSEMBLIES CENTRAL CLUSTER AND SYNCHRONISED PERTURBATION OF
COOLANT THERMAL-HYDRAULIC PARAMETERS.

Scenario	Combination of perturbations	ID
5	Temperature (5) & flow (6)	0 0 1 1
6	5×5 FA (2) & temperature (5)	1 0 1 0
7	5×5 FA (1) & temperature (5)	1 0 1 0
8	5×5 FA (4) & temperature (5)	0 1 1 0
9	5×5 FA (3) & temperature (5)	0 1 1 0
10	5×5 FA (2) & flow (6)	1 0 0 1
11	5×5 FA (1) & flow (6)	1 0 0 1
12	5×5 FA (4) & flow (6)	0 1 0 1
13	5×5 FA (3) & flow (6)	0 1 0 1

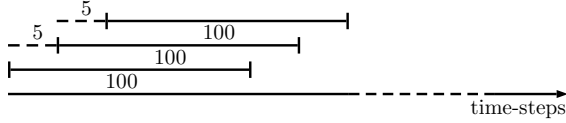


Fig. 4. Signal sampling. Signal windows of 100 time-steps were sampled using sliding windows of stride 5 time-steps

IV. THE PROPOSED APPROACH

A. Frequency Domain

Given complex reactor signals in the form of voxels, it is advantageous to capture spatial information in not only 2D coordinate space (i, j) but also channel-wise through k . This means that knowledge learnt in a particular area of the voxel can generalise well to others. The generalisation property of CNNs is crucial, as it allows for a great reduction in the number of parameters when compared to fully-connected networks, without sacrificing performance. However, it is important to state that the signal voxels are not a measure of induced neutron noise over time, but rather a measured response in every (i, j, k) location within the core reactor at a given time t . Therefore, the input signal voxels are more closely related to MRI or CT scans rather than videos in terms of data format. 3D CNNs have been used extensively in the medical field for tumour and legion segmentation, as well as in action recognition tasks to a very good level of success [19]–[23]. In pursuance of optimal feature extraction in all dimensions of the reactor signal, a bespoke 3D CNN is proposed.

1) *Convolutional Neural Networks*: Convolutional Neural Networks (CNNs) [24] perform automatic feature extraction through a series of volume-wise convolutions and feature routing. For each convolutional layer, a resulting set of filters are learned to capture spatial patterns in given inputs. Deeper CNNs are capable of capturing complex hierarchical concepts, whereby more general and abstract concepts initiate from the stem of the network and become increasingly task specific in the final layers. The convolution operation in CNNs is significantly more efficient than dense matrix multiplication through sparse interactions and parameter sharing. Formally, in 3D CNNs one would compute a pre-activated value of a

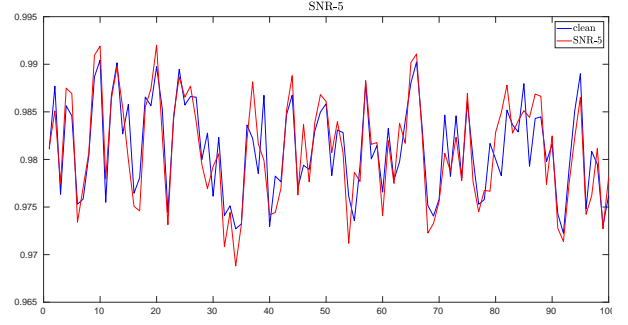


Fig. 5. Example of a signal obtained by means of S3K with noise added at $SNR = 5$.

given unit $n_{i,j,k}^{[\ell]}$ at (i, j, k) position in a 3D feature map of layer ℓ , by summing the weighted kernel contributions from the previous layer units in $\mathbf{A}^{[\ell-1]}$ as

$$n_{i,j,k}^{[\ell]} = \sum_{x=0}^{X-1} \sum_{y=0}^{Y-1} \sum_{z=0}^{Z-1} \mathbf{W}_{x,y,z}^{[\ell]} \mathbf{A}_{i+x,j+y,k+z}^{[\ell-1]} \quad (3)$$

where $\mathbf{W}_{x,y,z}^{[\ell]}$ is a single learned weight pertaining to a kernel $\mathbf{W}^{[\ell]}$ of dimensions $X \times Y \times Z$ in layer ℓ , which is convolved with cells from the previous layer ($\mathbf{W}^{[\ell]} * \mathbf{A}^{[\ell-1]}$). Each feature map f in a given layer ℓ has a learned bias term $b^{[\ell,f]}$, which is added pre non-linearity (σ) as $a_{i,j,k}^{[\ell,f]} = \sigma(n_{i,j,k}^{[\ell,f]} + b^{[\ell,f]})$.

Table V depicts the 3D-CNN architecture, devised through experimentation, for the classification of perturbation types in the frequency domain and their respective coordinate locations in 3D space. Convolutional layers use $3 \times 3 \times 3$ kernels with stride 1 and are followed by Batch Normalization and ReLU activations. In order to reduce the number of parameters incurred by 3D convolutions and increase the complexity of the network with more ReLU non-linearities, Bottleneck Layers ($1 \times 1 \times 1$ convolution) are introduced between $3 \times 3 \times 3$ convolutions. Max Pooling with $2 \times 2 \times 2$ kernels downsample inputs and a final Global Average Pooling layer produces 512 dimensional vector representations. The representations are then fed to 2 separate Fully-Connected Layers, one for multi-label classification with 3 sigmoid non-linear units and the other for perturbation coordinate regression (i, j, k) with 3 linear units.

In the Combined Perturbation case, the 3 sigmoid units can represent 7 different classes, denoted as a set $C = \{001, 010, 100, 101, 011, 110, 111\}$ containing all combinations of Localised (ID 100), Travelling type 1 (ID 010) and 2 (ID 001) perturbations as described in Section III. In practice, the 3 linear units become 9 units to allow for regression of more than one perturbation location at a time.

When training a CNN on multiple objectives, it is common practice to compute a linear weighted sum of losses per task i of T tasks, where weight coefficients λ_i control the dominance of each loss over the gradient. Formally, the multi-task optimisation objective is minimised with respect to \mathbf{W}

TABLE IV
3D-CNN ARCHITECTURE FOR FREQUENCY DOMAIN PERTURBATION
TYPE CLASSIFICATION AND SOURCE REGRESSION.

Input Size: 64×64×32×1		
Conv-BN-ReLU	3×3×3@64	64×64×32×64
MaxPool	2×2×2	32×32×16×64
Conv-BN-ReLU	1×1×1@32	32×32×16×32
Conv-BN-ReLU	3×3×3@128	32×32×16×128
MaxPool	2×2×2	16×16×8×128
Conv-BN-ReLU	1×1×1@64	16×16×8×64
Conv-BN-ReLU	3×3×3@256	16×16×8×256
MaxPool	2×2×2	8×8×4×256
Conv-BN-ReLU	1×1×1@128	8×8×4×128
Conv-BN-ReLU	3×3×3@512	8×8×4×512
MaxPool	2×2×2	4×4×2×512
4×4×2 Global Average Pooling		
3×1 Fully-Connected, Multi-sigmoid		
3×1 Fully-Connected, Linear		

parameters given \mathcal{D} input data as

$$\mathcal{L} = \sum_i^T \lambda_i \ell_i(\mathcal{D}; \mathbf{W}) \quad (4)$$

where ℓ_i represents the negative log likelihood loss for classification of the perturbation type (ℓ_1), or the L_2 loss for regressing the perturbation coordinates (ℓ_2). Concretely, the 3D-CNN is trained by minimising the following criterion

$$\begin{aligned} & -\frac{1}{N} \sum_{i=1}^N \left[\frac{\lambda_1}{P} \sum_{j=1}^P [y_j \log(\hat{y}_j) + (1 - y_j) \log(1 - \hat{y}_j)] \right. \\ & \quad \left. - \frac{\lambda_2}{C} \sum_{c=1}^C \|y_c - \hat{y}_c\|^2 \right] \end{aligned} \quad (5)$$

where P and C denote the number of perturbation types and location coordinates respectively, with λ_1 , λ_2 as tuned weight coefficients for each loss. The resulting network model $\mathcal{F}(\mathcal{D}; \mathbf{W})$ predicts a continuous vector of outputs (i, j, k coordinates) and discrete outputs for classes.

B. Time Domain

Given the sequential nature of the signals in the perturbation induced in the time domain, it was intuitive to utilise Recurrent Neural Networks (RNN). RNNs are particularly suitable for this type of data. Their cells can formulate a non linear output $a^{[t]}$ based on both the input data $x^{[t]}$ at the current time step t , and the previous time-step activation $a^{[t-1]}$, as described in (6), where h (i.e. hyperbolic tangent) is a non-linear activation function.

$$a^t = h(x^{[t]}, a^{[t-1]}) \quad (6)$$

In particular, Long Short-Term Memory (LSTM) was adopted because of its capability of learning long term dependencies on data. This is attained by formulating memory cells. The

equations relative to LSTM follow, and the reader is invited to refer to the original paper [25] for further details.

$$\begin{aligned} \tilde{c}^{[t]} &= \tanh(W_c[a^{[t-1]}, x^{[t]}] + b_c) \\ \Gamma_u &= \sigma(W_u[a^{[t-1]}, x^{[t]}] + b_u) \\ \Gamma_f &= \sigma(W_f[a^{[t-1]}, x^{[t]}] + b_f) \\ \Gamma_o &= \sigma(W_o[a^{[t-1]}, x^{[t]}] + b_o) \\ c^{[t]} &= \Gamma_u \odot \tilde{c}^{[t]} + \Gamma_f \odot \tilde{c}^{[t-1]} \\ a^{[t]} &= \Gamma_o \odot c^{[t]} \end{aligned} \quad (7)$$

In (7), c is the memory cell, Γ_u , Γ_f and Γ_o are the update, forget and output gates respectively; W denotes the model's weights, and b are bias vectors. These parameters are all jointly learned through back-propagation. Essentially, at each time-step, a candidate update of the memory cell is proposed (i.e. $\tilde{c}^{[t]}$), and based on the gates Γ , $\tilde{c}^{[t]}$ can be utilised to update the memory cell ($c^{[t]}$), and subsequently provide a non linear activation of the LSTM cell ($a^{[t]}$). To learn a meaningful representation of the signal, two LSTMs were stacked, both with 512 neurons. The problem of recognising which scenario a signal is representative of was tackled as a multi-label classification task. Since four individual perturbation (and their combinations) were identified (see Table I, II and III), in order to classify which of these perturbation was present, 512-dimensional LSTM representations were fully connected to four neurons with sigmoid activations.

C. Deep Time-Frequency Framework

As illustrated in Fig. 1, a Deep Neural Network framework was formulated for processing both Time and Frequency Domain signals coming from Nuclear Reactor sensor measurements. Both the 3D-CNN and LSTM network produce 512 dimensional vector representations of their respective inputs. The representations are then fed to a fused classification layer comprised of 7 sigmoid units (3 for Frequency & 4 for Time) to accommodate all scenario combinations as a multi-label classification task. Lastly, whenever a frequency domain perturbation is detected, the red switch in Fig. 1 is triggered and the current 512 dimensional representation is fed to a separate fully-connected layer to regress perturbation coordinates (i, j, k) in 3D space.

V. EXPERIMENTAL STUDY

A. Frequency Domain

For completeness and more detailed analysis of the results, the performance of the proposed framework in the Time and Frequency domain are kept separate. The results of the experiments conducted on the volumetric signal data are reported in Table V. As explained in greater detail in Subsection III-A, the volumetric signals were corrupted by obscuring parts (setting values to zero) at random, in order to emulate fewer available sensor measurements and thus increase the complexity of the problem.

In the first experiment (Keep20%), a dataset with 20% of the sensor measurements was generated. Similarly, in the second experiment (Keep5%) a different dataset was generated in which only 5% of the sensor measurements were kept. Both of

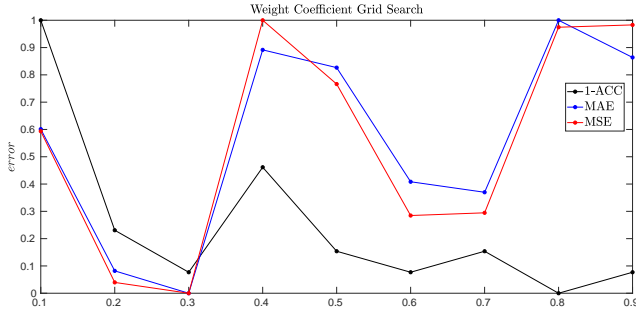


Fig. 6. Weight coefficient grid search for the 3D-CNN classification and regression losses. Coefficient 0.3 for classification and 0.7 for regression yielded the best performance.

these experiments were conducted to study the effect of sensor measurement sparsity on the performance of our algorithm. Furthermore, different training/validation and test splits were also utilised to study the effect of learning from a smaller pool of possible perturbations in the training set.

In the case of the Combined Perturbation experiments, a similar approach was undertaken with regards to the percentage of sensors kept and the dataset splits. Two datasets were generated for training (CombinedKeep20% and CombinedKeep5%) in which multiple perturbations are classified and their respective source coordinates regressed simultaneously. A grid search was performed to find the loss weight coefficients for each task, and the best results were achieved with $\lambda_1 = 0.3$ and $\lambda_2 = 0.7$ (see Fig. 6). For all experiments, the 3D-CNN was trained to minimise the criterion in Eq. (5) using backpropagation, and the Adam Optimiser [26] with the default parameters and batch size 32. Each model was trained 10 times and the mean performance was taken as the final result, along with the standard deviation. As observable in Table V, high classification performance was achieved in all experiments with $99.75\% \pm 0.09$ and $97.15\% \pm 0.15$ accuracy in the best case and worst case respectively. The mean squared and absolute errors (MSE, MAE) were used as evaluation metrics for the perturbation coordinate regression results, with best case of 0.2528 ± 0.03 (MAE), 0.1347 ± 0.02 (MSE) and worst case of 1.95 ± 0.11 (MAE), 11.90 ± 0.66 (MSE).

Overall, the results show that the classification task achieves better performance across all datasets compared to the regression task. The regression performance deteriorates with the introduction of combined perturbations and limited sensor measurement/training set size, whereas the classification of perturbations types is more resilient to fluctuations in the number of sensors used in the training phase.

B. Time Domain

In this experiment, individual sensor measurements were utilised to detect each of the thirteen scenarios (Table I, II and III). Starting with the data from the thirteen scenarios provided by S3K, each comprised of 56 one-dimensional signals of length 10001 (one signal per detector), after re-sampling, 17164 samples of size 56×100 were obtained.

TABLE V
3D-CNN ARCHITECTURE FOR FREQUENCY DOMAIN PERTURBATION TYPE CLASSIFICATION AND SOURCE REGRESSION.

Dataset	Split %	Accuracy	MAE	MSE
Keep20%	60/15/25	99.75 ± 0.09	0.2528 ± 0.03	0.1347 ± 0.02
	25/15/60	99.12 ± 0.17	0.4221 ± 0.05	0.4152 ± 0.07
	15/25/60	98.62 ± 0.22	0.5886 ± 0.05	0.8174 ± 0.12
Keep5%	60/15/25	99.32 ± 0.18	0.326 ± 0.05	0.2086 ± 0.04
	25/15/60	98.34 ± 0.22	0.4818 ± 0.05	0.6044 ± 0.08
	15/25/60	97.27 ± 0.54	0.689 ± 0.1	1.0749 ± 0.25
Combined Keep20%	60/15/25	99.82 ± 0.05	0.5602 ± 0.04	1.6036 ± 0.15
	25/15/60	99.56 ± 0.07	0.8942 ± 0.04	3.5739 ± 0.16
	15/25/60	99.44 ± 0.08	0.9635 ± 0.06	4.2814 ± 0.19
Combined Keep5%	60/15/25	99.47 ± 0.03	0.8809 ± 0.04	3.4424 ± 0.16
	25/15/60	98.33 ± 0.24	0.5001 ± 0.04	0.6381 ± 0.08
	15/25/60	97.15 ± 0.15	1.9528 ± 0.11	11.902 ± 0.66

Subsequently, each 56×100 sample was subdivided into 56 one-dimensional signals of size 100×1 . During training, each 100×1 signal from a single sensor was utilised to detect the presence of a scenario. In other words, any given scenario (perturbation) must be detected within one second of monitoring. Fig. 7 shows which sensors were utilised to train, validate and test the LSTM network, at each radial level of the reactor. Overall, 480592 (from 28 sensors), 240296 (from 14 sensors) and 240296 (from 14 sensors) signals were used for training, validating and testing.

Hyper-parameters were experimentally defined, and those utilised provided the best performance. Mini-batch stochastic gradient descent (with batch size 32) and cross-entropy loss (8) with Adam optimisation algorithm with default parameters were utilised for training.

$$\mathcal{L} = -\frac{1}{N \times P} \sum_{j=1}^P \sum_{i=1}^N [y_j \log(\hat{y}_j) + (1 - y_j) \log(1 - \hat{y}_j)]_i \quad (8)$$

In (8), P is the number of sigmoid units used for the multi-label classification task, N is the number of samples. The implementation was based on MATLAB [27], Keras deep learning framework [28] and Tensorflow numerical computation library [29]. The experiments were conducted using a server with an Intel Xeon(R) E5-2620 v4 CPU, eight GPUs and 96GB of RAM. The performance achieved by the LSTM was 0.97 on the clean signals, 0.81 with added noise at $SNR = 10$, 0.77 with added noise at $SNR = 5$.

VI. CONCLUSION & FUTURE WORK

In this paper, the first step towards a unified deep framework was proposed for the classification and regression of perturbations in nuclear reactors. Both time and frequency domain data were obtained through inducing perturbations such as an absorber of variable strength in and propagating perturbation in the frequency domain, vibration of fuel assemblies in the time domain and fluctuations of thermal-hydraulic parameters at the inlet coolant between the 4-loops of a Westinghouse PWR reactor.

The proposed framework is comprised of a 3D-CNN and an LSTM architecture that output 512-dimensional represen-

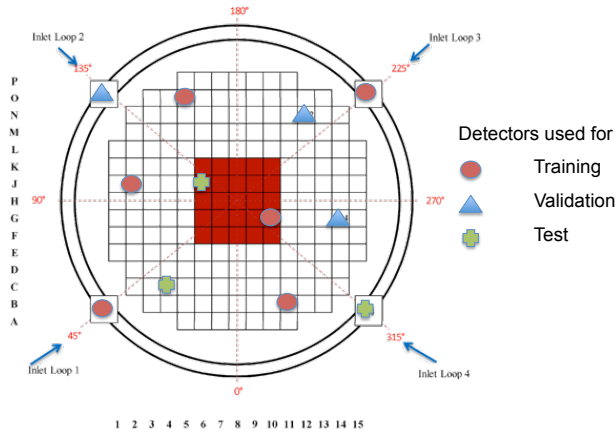


Fig. 7. Description of detectors utilised for training, validation and testing of the LSTM model.

tations of their respective input signals, and combinations of nuclear reactor perturbations are classified in a fused multi-sigmoid layer. A switch was introduced to control the flow of the frequency domain 512-dimensional representation, which is fed to a regression layer whenever a perturbation is detected in the 3D signal volume. Furthermore, the effects of sensor measurement sparsity and noisy signals were evaluated in a series of experimental studies, demonstrating the capability of our framework to achieve good results in both unfolding and classifying perturbation types.

In our future work, we will extend our studies to other types of simulated and/or real-life data coming from nuclear power plants, in pursuit of a framework suitable for simultaneously handling of Time and Frequency domain signals for the localisation and classification of nuclear reactor anomalies.

ACKNOWLEDGMENT

The research conducted was made possible through funding from the Euratom research and training programme 2014-2018 under grant agreement No 754316 for the 'CORE Monitoring Techniques And EXperimental Validation And Demonstration (CORTEX)' Horizon 2020 project, 2017-2021.

REFERENCES

- [1] Francesco Caliva, Fabio De Sousa Ribeiro, Antonios Mylonakis, Christophe Demazière, Paolo Vinai, Georgios Leontidis, Stefanos Kollias, et al. A deep learning approach to anomaly detection in nuclear reactors. *Neural Networks (IJCNN)*, 2018 IEEE International Joint Conference on, 2018.
- [2] X. Jin, Y. Guo, S. Sarkar, A. Ray, and R. M. Edwards. Anomaly detection in nuclear power plants via symbolic dynamic filtering. *IEEE Transactions on Nuclear Science*, 58(1):277–288, Feb 2011.
- [3] Salman Zaferanlouei, Dariush Rostamifard, and Saeed Setayeshi. Prediction of critical heat flux using anfis. *Annals of Nuclear Energy*, 37(6):813 – 821, 2010.
- [4] Wei Li, Min jun Peng, Ming Yang, Geng lei Xia, Hang Wang, Nan Jiang, and Zhan guo Ma. Design of comprehensive diagnosis system in nuclear power plant. *Annals of Nuclear Energy*, 109:92 – 102, 2017.
- [5] T.V. Santosh, A. Srivastava, V.V.S. Sanyasi Rao, A.K. Ghosh, and H.S. Kushwaha. Diagnostic system for identification of accident scenarios in nuclear power plants using artificial neural networks. *Reliability Engineering and System Safety*, 94(3):759 – 762, 2009.
- [6] Farhan Jamil, Muhammad Abid, Inamul Haq, Abdul Qayyum Khan, and Masood Iqbal. Fault diagnosis of pakistan research reactor-2 with data-driven techniques. *Annals of Nuclear Energy*, 90:433 – 440, 2016.
- [7] Dimitrios Kollias, Miao Yu, Athanasios Tagaris, Georgios Leontidis, Andreas Stafylopatis, and Stefanos Kollias. Adaptation and contextualization of deep neural network models. In *2017 IEEE Symposium Series on Computational Intelligence (SSCI)*, pages 1–8, 2017.
- [8] Fabio De Sousa Ribeiro, Francesco Caliva, Mark Swainson, Kjartan Gudmundsson, Georgios Leontidis, and Stefanos Kollias. An adaptable deep learning system for optical character verification in retail food packaging. In *Evolving and Adaptive Intelligent Systems, IEEE International Conference on*, 2018.
- [9] Jason Yosinski, Jeff Clune, Yoshua Bengio, and Hod Lipson. How transferable are features in deep neural networks? In *Advances in neural information processing systems*, pages 3320–3328, 2014.
- [10] Dimitrios Kollias, Athanasios Tagaris, Andreas Stafylopatis, Stefanos Kollias, and Georgios Tagaris. Deep neural architectures for prediction in healthcare. *Complex & Intelligent Systems*, pages 1–13, 2018.
- [11] Alex Krizhevsky, Ilya Sutskever, and Geoffrey E Hinton. Imagenet classification with deep convolutional neural networks. In *Advances in neural information processing systems*, pages 1097–1105, 2012.
- [12] Andrej Karpathy, George Toderici, Sanketh Shetty, Thomas Leung, Rahul Sukthankar, and Li Fei-Fei. Large-scale video classification with convolutional neural networks. In *Proceedings of the IEEE conference on Computer Vision and Pattern Recognition*, pages 1725–1732, 2014.
- [13] Fabio De Sousa Ribeiro, Liyun Gong, Francesco Caliva, Kjartan Gudmundsson, Mark Swainson, Miao Yu, Georgios Leontidis, Xujiong Ye, Stefanos Kollias, et al. An end-to-end deep neural architecture for optical character verification and recognition in retail food packaging. In *Image Processing, IEEE International Conference on (ICIP)*, 2018.
- [14] F. C. Chen and M. R. Jahanshahi. Nb-cnn: Deep learning-based crack detection using convolutional neural network and naïve bayes data fusion. *IEEE Transactions on Industrial Electronics*, 65(5):4392–4400, May 2018.
- [15] Christophe Demazière. Core sim: a multi-purpose neutronic tool for research and education. *Annals of Nuclear Energy*, 38(12):2698–2718, 2011.
- [16] Christophe Demazière. User's manual of the core sim neutronic tool. Technical report, Chalmers University of Technology, 2011.
- [17] Tomasz Kozłowski and Thomas J Downar. Oecd/nea and us nrc pwr mox/uo2 core transient benchmark. *Final Specifications, Revision*, 2, 2003.
- [18] G Grandi, JA Borkowsky, and KS Smith. Simulate-3k models and methodology. *SSP-98013, Revision*, 6, 2006.
- [19] Konstantinos Kamnitsas, Christian Ledig, Virginia FJ Newcombe, Joanna P Simpson, Andrew D Kane, David K Menon, Daniel Rueckert, and Ben Glocker. Efficient multi-scale 3d cnn with fully connected crf for accurate brain lesion segmentation. *Medical image analysis*, 36:61–78, 2017.
- [20] Özgün Çiçek, Ahmed Abdulkadir, Soeren S Lienkamp, Thomas Brox, and Olaf Ronneberger. 3d u-net: learning dense volumetric segmentation from sparse annotation. In *International Conference on Medical Image Computing and Computer-Assisted Intervention*, pages 424–432. Springer, 2016.
- [21] Shuiwang Ji, Wei Xu, Ming Yang, and Kai Yu. 3d convolutional neural networks for human action recognition. *IEEE transactions on pattern analysis and machine intelligence*, 35(1):221–231, 2013.
- [22] Daniel Maturana and Sebastian Scherer. Voxnet: A 3d convolutional neural network for real-time object recognition. In *Intelligent Robots and Systems (IROS), 2015 IEEE/RSJ International Conference on*, pages 922–928. IEEE, 2015.
- [23] Fausto Milletari, Nassir Navab, and Seyed-Ahmad Ahmadi. V-net: Fully convolutional neural networks for volumetric medical image segmentation. In *3D Vision (3DV), 2016 Fourth International Conference on*, pages 565–571. IEEE, 2016.
- [24] Yann LeCun et al. Generalization and network design strategies. *Connectionism in perspective*, pages 143–155, 1989.
- [25] Sepp Hochreiter and Jürgen Schmidhuber. Long short-term memory. *Neural computation*, 9(8):1735–1780, 1997.
- [26] Diederik Kingma and Jimmy Ba. Adam: A method for stochastic optimization. *arXiv preprint arXiv:1412.6980*, 2014.
- [27] MATLAB Users Guide. The mathworks. Inc., Natick, MA, 5:333, 1998.
- [28] François Chollet et al. Keras, 2015.

- [29] Martín Abadi, Paul Barham, Jianmin Chen, Zhifeng Chen, Andy Davis, Jeffrey Dean, Matthieu Devin, Sanjay Ghemawat, Geoffrey Irving, Michael Isard, et al. Tensorflow: a system for large-scale machine learning. In *OSDI*, volume 16, pages 265–283, 2016.